iScience

CellPress
OPEN ACCESS

Article

Hydra vulgaris shows stable responses to thermal stimulation despite large changes in the number of neurons

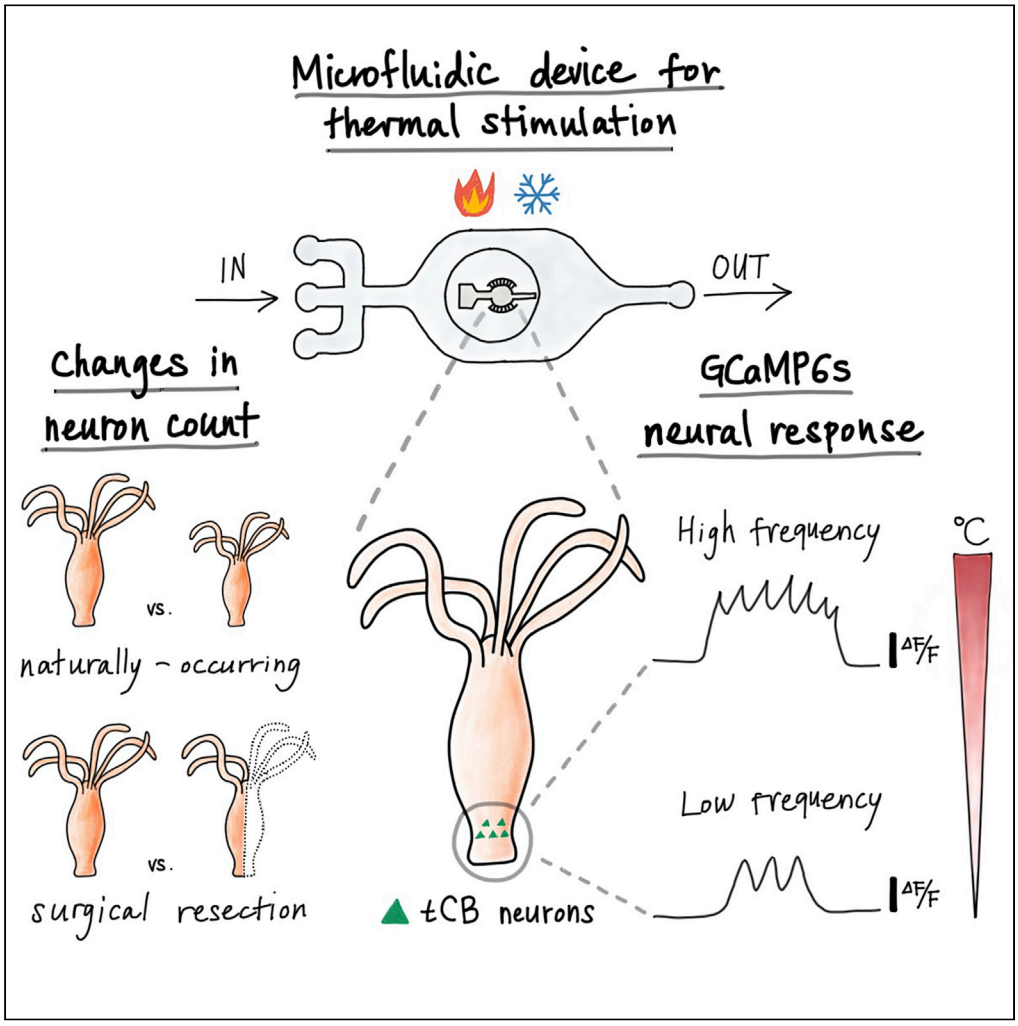

Constantine N. Tzouanas, Soonyoung Kim, Krishna N. Badhiwala, Benjamin W. Avants, Jacob T. Robinson

jtrobinson@rice.edu

Highlights

Thermal stimulation drives temperature-dependent firing rate in specific *Hydra* neurons

Hydra show stable neural responses to temperature despite 2× decrease in neuron count

Injury tolerance of *Hydra* offers model for stable neural architecture

Tzouanas et al., iScience *24*, 102490
June 25, 2021
https://doi.org/10.1016/j.isci.2021.102490

iScience

CellPress
OPEN ACCESS

Article

Hydra vulgaris shows stable responses to thermal stimulation despite large changes in the number of neurons

Constantine N. Tzouanas,[1,4,5] Soonyoung Kim,[2,4] Krishna N. Badhiwala,[1] Benjamin W. Avants,[2] and Jacob T. Robinson[1,2,3,6,*]

SUMMARY

Many animals that lose neural tissue to injury or disease can maintain behavioral repertoires by regenerating new neurons or reorganizing existing neural circuits. However, most neuroscience small model organisms lack this high degree of neural plasticity. We show that *Hydra vulgaris* can maintain stable sensory-motor behaviors despite 2-fold changes in neuron count, due to naturally occurring size variation or surgical resection. Specifically, we find that both behavioral and neural responses to rapid temperature changes are maintained following these perturbations. We further describe possible mechanisms for the observed neural activity and argue that *Hydra*'s radial symmetry may allow it to maintain stable behaviors when changes in the numbers of neurons do not selectively eliminate any specific neuronal cell type. These results suggest that *Hydra* provides a powerful model for studying how animals maintain stable sensory-motor responses within dynamic neural circuits and may lead to the development of general principles for injury-tolerant neural architectures.

INTRODUCTION

One remarkable feature of the nervous system is plasticity, the ability to alter or reorganize neural circuits to gain or restore function, particularly in response to injury. In mammals, individual neurons can alter their excitability based on presynaptic transmission frequencies to maintain stable activity levels (Turrigiano, 2008). Deficits in this process of homeostatic plasticity have been associated with neural disorders (Tatavarty et al., 2020). Synaptic plasticity at the circuit level allows collections of neurons to remap connections. This produces behavioral compensation after broad injuries such as strokes and uses molecular mechanisms similar to those involved in neural development (Murphy and Corbett, 2009). Non-mammalian animals, such as salamanders and crustaceans, can regenerate limbs and their associated peripheral nerves (Alwes et al., 2016; Joven et al., 2019), whereas the cnidarian polyp *Hydra vulgaris* can regrow its entire body and complete nervous system from a fragment as small as ~300 cells (Shimizu et al., 1993). A major challenge in understanding how neural plasticity supports and maintains animal behavior during nervous system regeneration is the difficulty in observing complete neural activity during reorganization.

Millimeter-sized invertebrates are ideal model systems for studying neural plasticity and recovery from injury because they have relatively small nervous systems amenable to live imaging of neural circuit reorganization. However, most small invertebrate model organisms either show modest neural regeneration or lack well-developed transgenic techniques. For instance, neurons in the central nervous system of *Drosophila* do not regenerate following axotomies in either whole-brain cultures (Ayaz et al., 2008) or larvae (Song et al., 2012). In *C. elegans*, axons of select neurons can regenerate after being severed (Yanik et al., 2004); however, growth trajectories are error prone (Wu et al., 2007) even when identical neurons across animals are subjected to similar injury protocols (Hammarlund and Jin, 2014). Exceptional neural plasticity can be found in planarians, which regenerate entire organisms (Massobrio et al., 2015) from small fragments of tissue, but these animals lack a suite of transgenic tools similar to that of *Drosophila* and *C. elegans* (Scimone et al., 2017).

Hydra vulgaris is unique among invertebrate model organisms in that it is amenable to a variety of transgenic techniques and displays remarkable regenerative capabilities. These regenerative abilities include

[1]Department of Bioengineering, Rice University, 6100 Main Street, Houston, TX 77005, USA

[2]Department of Electrical and Computer Engineering, Rice University, 6100 Main Street, Houston, TX 77005, USA

[3]Department of Neuroscience, Baylor College of Medicine, One Baylor Plaza, Houston, TX 77030, USA

[4]These authors contributed equally

[5]Present address: Institute for Medical Engineering & Science, Massachusetts Institute of Technology, 45 Carleton Street, Cambridge, MA 02139, USA.

[6]Lead contact

*Correspondence: jtrobinson@rice.edu

https://doi.org/10.1016/j.isci.2021.102490

complete regeneration of the entire organism from fragments of only a few hundred cells (Shimizu et al., 1993; Technau et al., 2000), and its entire nervous system can be rebuilt from a single interstitial stem cell (David and Murphy, 1977). The robustness of *Hydra*'s nervous system arises from its constitutively active multipotent interstitial stem cells, which give rise to several cell types, including neurons. In an uninjured, homeostatic animal, all differentiated cell types, including neurons, are continually shed and replaced every 20 days by stem cells (Campbell, 1967). This results in the continual differentiation of neurons in an adult animal, and thus the continual remodeling of existing neural circuits to account for the loss and gain of neurons. Likewise, *Hydra*'s radial symmetry offers opportunities to experimentally modulate the number of neurons while preserving the presence of cell types. For example, when cut along the oral-aboral axis, we expect that the remaining tissue will have cells from all neuronal cell types. Thus, when the animal reseals its body column, its radially symmetric neural structure can be preserved while containing fewer total neurons. These properties of the *Hydra* nervous system make it an excellent model to study how new neurons integrate into existing circuits and how neuronal circuits are rebuilt following injury.

The small size and genetic tractability of *Hydra* provide additional advantages. As a millimeter-scale invertebrate, an entire *Hydra* can be imaged at a single-cell resolution (Dupre and Yuste, 2017). Furthermore, the ability to generate transgenic lines by embryo injection (Wittlieb et al., 2006; Juliano et al., 2014) has enabled functional calcium imaging in neurons (Dupre and Yuste, 2017) and epitheliomuscular cells (Szymanski and Yuste, 2019). In addition, cell-type specific promoters have been identified using single-cell transcriptomic analysis of the *Hydra* nervous system. These data reveal that *Hydra* has 12 neuronal subtypes, each expressing distinct sets of biomarkers linked to neuronal development and function (Noro et al., 2019; Siebert et al., 2019).

Given *Hydra's* potential as a model for neural regeneration and plasticity, it is critical to establish behavioral assays that indicate if and when neural circuits have regained their ability to regulate behavior. Although *Hydra* has been studied for over 300 years, we lack quantitative characterization of behaviors like sensory-motor responses. Studies of behavior dating back to the 1700s (Campbell, 2008) qualitatively describe responses to light (Passano and McCullough, 1963), chemicals (Kepner and Hopkins, 1924), and temperature (Mast, 1903; Schroeder and Callaghan, 1981; Bosch et al., 1988), but these experiments fall short of quantitative evaluation of behavior and neural activity. Recently, machine learning approaches have been used to identify behavioral motifs in freely moving *Hydra*, but these experiments have not been extended to sensory-motor responses (Han et al., 2018).

Hydra's response to a rapid change in temperature is one sensory-motor behavior that could be used to assess neural plasticity, but this behavior must first be quantified. Although prior experiments suggest that *Hydra* can sense and react to temperature, more work is needed to precisely demonstrate and quantify the animal's neural and behavioral response patterns to a rapid temperature change. Mast showed that when touched by heated objects, *Hydra* responds by bending toward the stimulus, but these experiments cannot fully distinguish between mechanosensory and thermosensory behaviors (Mast, 1903). Schroeder and Callaghan reported the highest and lowest temperatures in which *Hydra oligactis* and *Hydra pseudoligactis* could survive (Schroeder and Callaghan, 1981). Bosch et al. demonstrated that exposing *Hydra* to moderately elevated temperatures (30°C for two hours) increases their ability to survive culture at high temperatures (34°C for 4 days) that would otherwise be lethal (Bosch et al., 1988). Yamamoto and Yuste likewise found that extended exposure to elevated temperatures did not affect various behavioral features in *Hydra*, including long-term contraction burst frequency and detachment events (Yamamoto and Yuste, 2020). These experiments show that *Hydra*'s viability depends on the ambient temperature and that *Hydra* can adapt to elevated environmental temperatures, but they do not reveal the specific sensory-motor response and neural processing of an acute thermal stimulus.

Here we show the first quantitative description of *Hydra*'s behavioral and neural response to acute thermal stimulation. We demonstrate that these responses are maintained even if the number of neurons in the animal changes by a factor of 2 due to surgery or naturally occurring variation in animal size, assuming that there is no complete loss of any particular neural cell type. To perform this study, we developed a microfluidic device capable of delivering rapid and precise thermal stimuli without the confounding effect of mechanical stimulation. Using this technique, we find that *Hydra* elongates after the onset of positive thermal stimulation, followed by contraction. Synchronous with body movements, we find temperature-related oscillatory neural activity within a ring of neurons in *Hydra*'s peduncle. The frequency of this oscillation

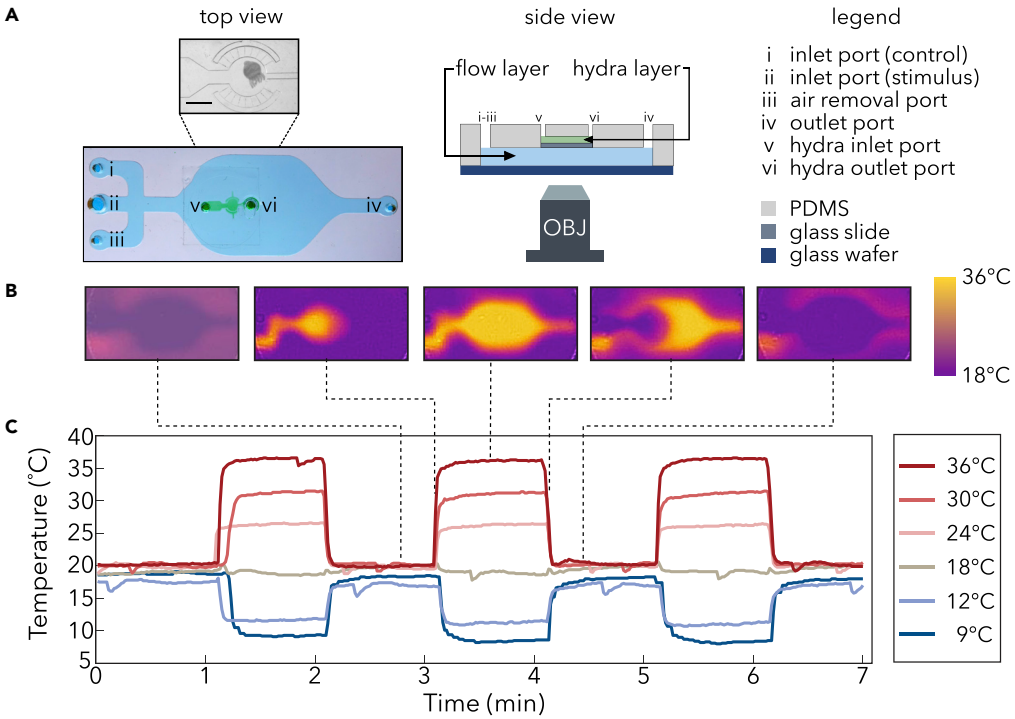

Figure 1. Characterization and validation of two-layer microfluidic device for thermal stimulation of *Hydra vulgaris*

(A) (Left) Photograph of microfluidic device with blue dye in flow layer and green dye in *Hydra* chamber. Scale bar, 1 mm. (Middle) Schematic of cross-section of the device. (Right) Legend for left and middle panels.

(B) Infrared image showing temperature of the flow layer before (leftmost), the start of (second leftmost), during (center), end of (second rightmost), and after (rightmost) thermal stimulation.

(C) Time course of thermal stimulation at temperatures above and below *Hydra*'s baseline culture temperature of 18°C.

decreases for negative thermal stimulation (i.e., cooling) and increases for positive thermal stimulation (i.e., heating). We show that the frequency of the neural oscillation varies with the absolute temperature of the thermal stimuli, rather than relative changes from culture temperature. Importantly, we find that these oscillation frequencies are nearly unchanged even if the number of neurons in these animals changes by a factor of 2, whether due to surgical resectioning or natural size variation. Overall, these data describe a specific sensory-motor behavior and associated neural activity that is robust to large changes in the number of neurons in this animal.

RESULTS

Microfluidic device enables thermal stimulation and whole-body imaging of *Hydra vulgaris*

Because *Hydra* are sensitive to mechanical stimulation (e.g., touch and changes in fluid flow [Rushforth et al., 1963; Passano and McCullough, 1964; Khetan et al., 2018]), we designed a two-layer microfluidic device to deliver thermal stimuli without mechanical confounds: a *Hydra* immobilization chamber fabricated above a flow layer with multiple inlet ports (Figure 1A, see transparent methods). By connecting the flow layer's inlet ports to in-line heaters at different temperature setpoints, we can provide rapid and precise thermal stimulation by switching fluid flow through the different inlet ports—a process that we automate using microcontrollers (see transparent methods). In our experiments, one inlet (i in Figure 1A) provides fluid that is maintained at *Hydra*'s culture temperature to serve as a control. A second inlet provides fluid that is maintained at a stimulus temperature ranging from 9°C to 36°C. To validate our ability to rapidly and repeatedly modulate the temperature of the *Hydra* immobilization chamber, we measured the temperature of the device glass with an infrared camera (Figures 1B and 1C). We found that the temperature plateaus in approximately 5 s after the start of the temperature change and that the temperature set points were repeatable to within a standard deviation of 0.5°C across multiple stimulation cycles.

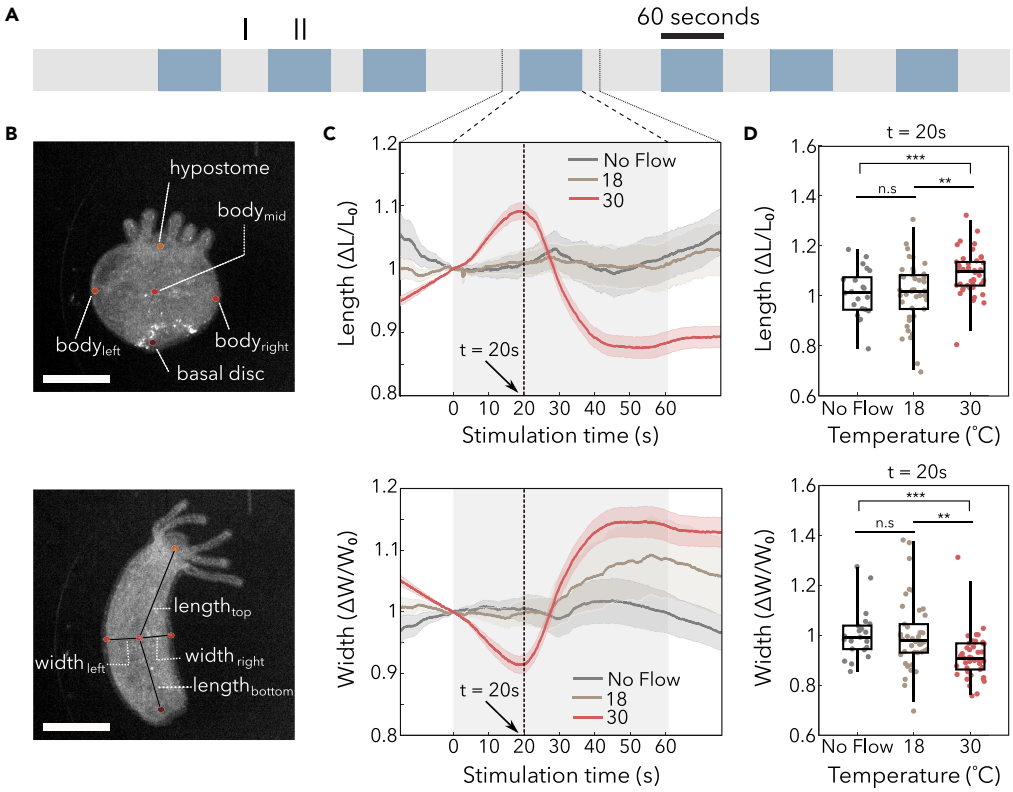

Figure 2. *Hydra*'s body length initially increases and width initially decreases when stimulated at 30°C

(A) Schematic of a representative thermal stimulation protocol. Gray regions (I) indicate non-stimulus periods at *Hydra*'s culture temperature lasting between 30 and 90 s, and blue-colored regions (II) indicate stimulus periods at designated temperatures for 60 s.

(B) Representative frame annotated from DeepLabCut. Top panel describes which body points were annotated, and the bottom panel shows how the length and width of the animals are determined. The hypostome is the end of the body with *Hydra*'s mouth and tentacles (oral end), whereas the basal disc is used to adhere to substrates (aboral end). Scale bar, 500 μm.

(C) Average length and width of *Hydra* calculated for stimulation periods and time-aligned to stimuli, with 15 s before and after stimulation periods. Curve corresponds to mean, and shaded error bars correspond to standard error of the mean. N = 3 *Hydra* for No Flow, N = 6 *Hydra* for 18°C and 30°C.

(D) The change in length (top panel) and width (bottom panel) at 20 s after onset of stimulation (t = 20 s), for each stimulus period. Box-and-whisker plots indicate Q1, median, and Q3; whisker lengths indicate the 2nd and 98th percentiles. N = 3 *Hydra* for No Flow, N = 6 *Hydra* for 18°C and 30°C. (n.s = not significant, **p < 0.001, ***p < 0.0001, unpaired t test).

Positive thermal stimulation drives sequential elongation and contraction in *Hydra vulgaris*

Having fabricated a microfluidic device that allows us to thermally stimulate and simultaneously image *Hydra*, we supplied fluids of different temperatures to the flow layer to measure how *Hydra* responds to a rapid change in temperature. To avoid synchronizing thermal stimuli with natural rhythmic behavior (Passano and McCullough, 1964; Rushforth, 1971) or entraining a periodic response, we applied thermal stimuli for a period of 60 s and randomized the time interval between successive stimuli (Figure 2A). We quantified changes in *Hydra*'s posture by using DeepLabCut (Nath et al., 2019) to automate labeling of *Hydra*'s body width and length using hypostome (oral end), basal disc (aboral end), and the leftmost, middle, and rightmost points in the body column region (Figure 2B, see transparent methods). We observed no statistically significant changes to *Hydra*'s body length in experiments when we switched the source of the flow layer between two sources at 18°C compared with experiments with no fluid flow ("18°C" and "No flow" curves in Figure 2C), showing that the developed microfluidic device does not produce mechanical stimulation. However, we found that *Hydra* responds to a rapid change in temperature by first elongating and then longitudinally contracting. The peak body length occurs approximately 20 s after the stimulus onset (Figures 2C and 2D).

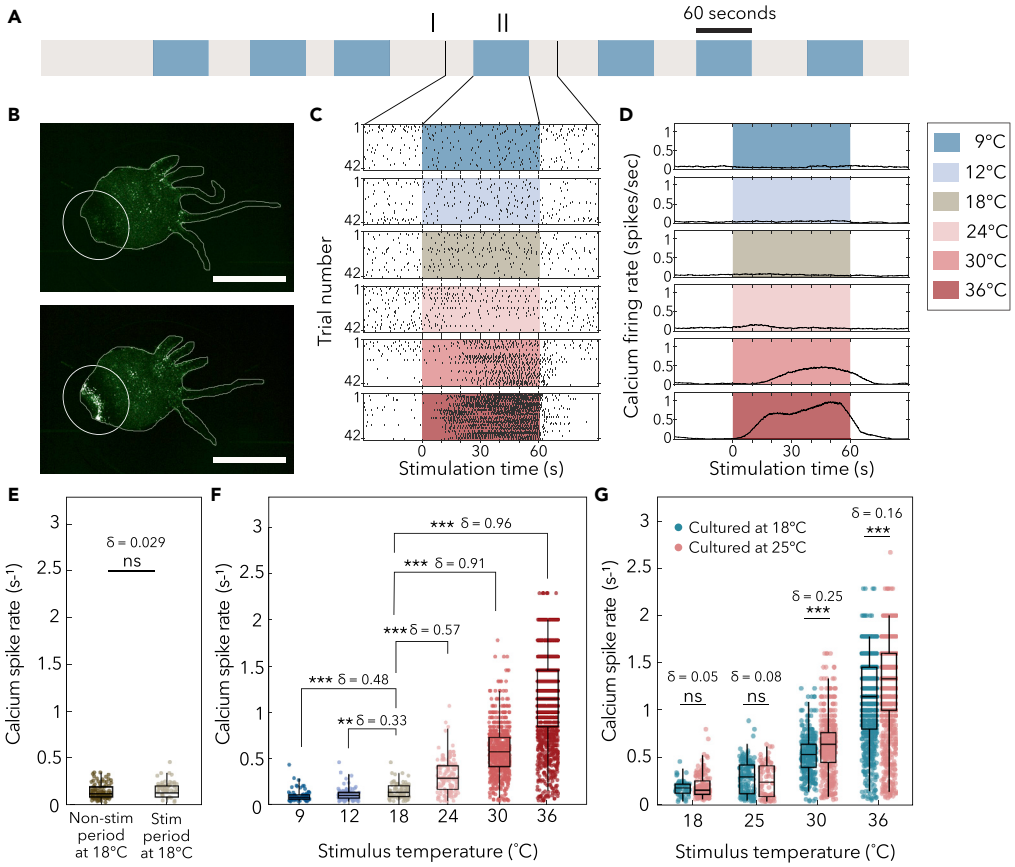

Figure 3. Thermal stimulation modulates the synchronous neural activity in the peduncle of *Hydra vulgaris*, see also Figures S1 and S2.

(A) Schematic of a representative thermal stimulation protocol. Gray-colored regions (I) indicate non-stimulus periods at *Hydra*'s culture temperature (either 18°C or 25°C) lasting between 30 and 90 s. The blue-colored regions (II) indicate stimulus periods at designated temperatures for 60 s.

(B) Images of *Hydra* without synchronous neural firing (top) and during firing (bottom) in the peduncle (white circle). Scale bar, 1 mm.

(C) Raster plot of synchronous firing events in peduncle in (B). One black vertical line indicates one synchronous firing event. Each row represents the raster plot of spikes time-aligned with one stimulation (boxed regions) with 30 s before and after stimulation (white non-boxed region).

(D) Peristimulus time histogram (calcium firing rate) of (C), which was calculated with a 10-s sliding window.

(E) Calcium spike rate comparison between the non-stimulation (gray-colored region I in A) and stimulation (blue-colored region II in A) periods with a stimulus temperature of 18°C. (ns = not significant, Mann-Whitney U test. δ = Effect size using Cliff's delta). Box-and-whisker plots indicate Q1, median, and Q3; whisker lengths indicate the 2nd and 98th percentiles.

(F) Calcium spike rates from *Hydra*, all cultured at 18°C. N = 6 animals per stimulus temperature. (ns = not significant, **p < 0.0001, ***p < 0.00001, Mann-Whitney U test. δ = Effect size using Cliff's delta). Box-and-whisker plots indicate Q1, median, and Q3; whisker lengths indicate the 2nd and 98th percentiles.

(G) Calcium spike rates from *Hydra* cultured at 18°C and 25°C. x axis notes the stimulation temperatures. N = 3 per culture temperature at each stimulation temperature. (ns = not significant, ***p < 0.00001, Mann-Whitney U test. δ = Effect size using Cliff's delta). Box-and-whisker plots indicate Q1, median, and Q3; whisker lengths indicate the 2nd and 98th percentiles.

Subset of peduncle neurons show periodic calcium spikes in response to thermal stimulation

Using fluorescence imaging of transgenic *Hydra* that express the calcium-sensitive fluorophore GCaMP6s in neurons, we observed bursts of synchronous calcium spikes following thermal stimulation in a group of neurons in the animal's peduncle (Figures 3A and 3B, Video S1, Video S2). We will refer to these neurons as temperature-linked contraction burst (tCB) neurons because their activity is closely linked to body contractions as described previously (Szymanski and Yuste, 2019) and are active following thermal stimulation. To

quantify the calcium spike rates in tCB neurons following thermal stimulation, we selected a region of interest (ROI) that encompassed the entire *Hydra* peduncle (Figure 3B). Although not all neurons in this region are putative tCB neurons, the strong signal produced by the synchronous tCB neuron activity allowed us to measure the collective synchronous calcium spike rate using this ROI (Figures 3C, 3D, and S1; Videos S1 and S2, see transparent methods). We found that *Hydra*'s calcium spike rate did not significantly change when switching between fluid reservoirs at 18°C, suggesting that changing fluids in the flow layer did not produce a mechanical stimulation artifact (Figure 3E, p value > 0.1, Cliff's delta effect size $\delta = 0.029$).

To estimate the population-level variability in calcium spike rates against which we could compare the response to thermal stimulation, we calculated the effect size of natural variation (Figures 3C–3G and S2). We subjected three organisms to identical temperature stimulation 48 h apart, finding that *Hydra* could exhibit significant day-to-day variability. For instance, one animal did not have statistically significant day-to-day variation in calcium spike rates (Figure S2, $p > 0.1$, $\delta = 0.04$), whereas another exhibited highly statistically significant differences in its neural responses to identical temperature stimulation on different days (Figure S2, $p < 0.0001$, $\delta = 0.61$). When day-to-day trials between the three organisms are aggregated based on the experimental day (analogous to Figure 3G), the collective difference between experimental days has an effect size of $\delta = 0.35$, providing an indication of day-to-day, random variation that can be expected from data collected across groups of *Hydra*. As a conservative measure for evaluating our experimental findings, $\delta = 0.61$ will be used for reference to day-to-day variation that is discussed hereafter. Because of *Hydra*'s day-to-day variability, we proceeded to interpret subsequent results based on both p values (for determining whether medians of calcium spike rate distributions are different) and effect size (as key context on the magnitude of experimentally induced changes in *Hydra*'s neural activity).

When we thermally stimulated *Hydra* across a wide range of temperatures both above and below their culture temperature, we observed that the tCB neurons' calcium spike rate during positive thermal stimulation (i.e., heating) was significantly higher than in control experiments (compare conditions labeled "24°C," "30°C," and "36°C" with the control condition of "18°C" in Figures 3C, 3D, and 3F). Likewise, tCB neurons' spike rate decreased during negative thermal stimulation (i.e., cooling; compare conditions labeled "9°C" and "12°C" with the control condition of "18°C" in Figures 3C, 3D, and 3F). We also found that the firing rate of the tCB neurons during thermal stimulation depends primarily on the absolute temperature of the thermal stimulus and not on the relative increase in temperature. When we increased the *Hydra* culture temperature from 18°C to 25°C, there was no significant change in the calcium spike rate for low thermal stimulus temperatures (i.e., stimulus at 18°C and 25°C in Figure 3G). At high stimulus temperatures (i.e., 30°C and 36°C in Figure 3G), we observed a statistically significant difference based on culture temperature, but the effect size was small compared with *Hydra*'s day-to-day variability ($\delta = 0.25$ at 30°C stimulation, $\delta = 0.16$ at 36°C stimulation, δ of up to 0.61 for identical stimulus on the same organism across different days). Furthermore, the effect size of changing *Hydra*'s culture temperature was small compared with changing the stimulation temperature by a comparable amount (e.g., $\delta = 0.71$ between *Hydra* stimulated at 30°C or 36°C, but both cultured at 18°C). These results support the conclusion that the calcium spike rate of tCB neurons depends primarily on the absolute temperature of a thermal stimulus, rather than relative changes from a culture temperature baseline.

Hydra vulgaris' neural response to thermal stimulation is robust against naturally-occurring 2-fold changes in neuron count

Having identified that the calcium spike rate of tCB neurons correlates with the absolute temperature of a thermal stimulus, we asked if this relationship is maintained even if the animals have significantly different numbers of neurons. To answer this question, we first determined that the number of neurons in *Hydra* is linearly related to the size of the animal. Using longitudinal fluorescence imaging of *Hydra* over 2 weeks of starvation or regular feedings (see transparent methods), we found that the number of neurons scaled with *Hydra*'s body volume regardless of how that body volume was reached (e.g., small organism by food deprivation versus small organism due to recent budding), consistent with prior reports of the density of neurons as a function of animal size (Bode et al., 1973; Otto and Campbell, 1977; Siebert et al., 2019) (Figures 4A–4C). Given the gradual change in body size over the time course of days, we expect that neuronal subtypes and structures will be preserved, despite changes in the total number of neurons.

To compare the thermal responses of animals with different sizes, we separated animals into "large" and "small" cohorts according to their body size (area calculated through binarization of *Hydra* images). Based

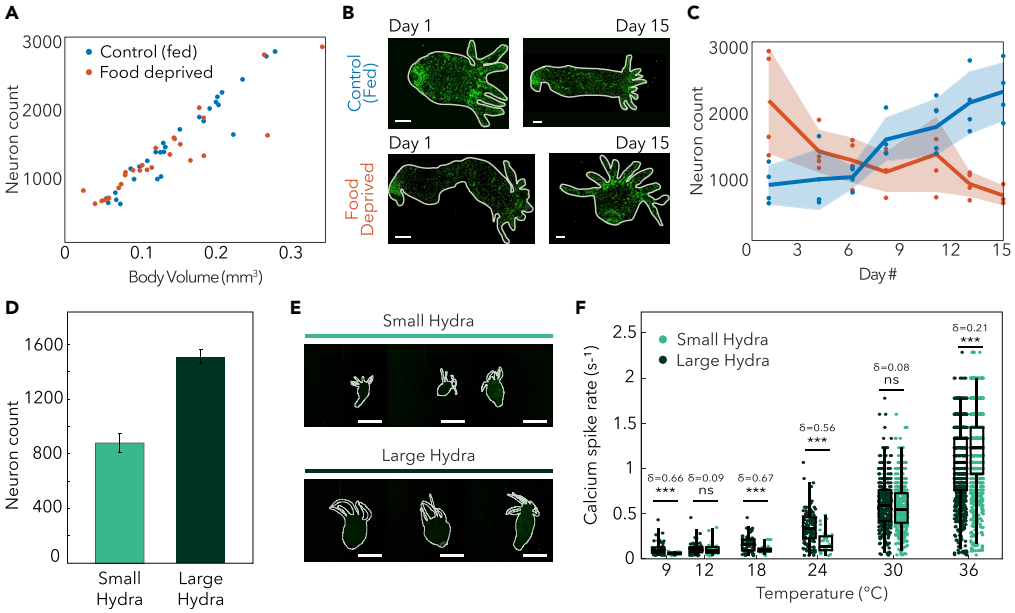

Figure 4. Calcium spike rate of tCB neurons does not depend on *Hydra*'s body size and number of neurons, see also Figure S3

(A) Number of neurons as a function of animal size (N = 4 per diet condition).

(B) Fluorescence images of *Hydra* at days 1 and 15 for both control and food-deprived groups (pseudo colored). Scale bar, 200 μm.

(C) Change in the number of neurons over the time course of 15 days. Curve corresponds to the mean, and shaded region corresponds to standard deviation.

(D) Estimated number of neurons from measurements in (A). Data represented as mean ± standard error of the mean.

(E) Three representative *Hydra* from small and large groups (pseudo colored). Scale bar, 1 mm.

(F) Calcium spike rates from large (N = 3 per size at each temperature) and small (N = 3 per size at each temperature) *Hydra*, all cultured at 18°C. (ns = not significant, ***p < 0.00001, Mann-Whitney U test. δ = Effect size using Cliff's delta). Box-and-whisker plots indicate Q1, median, and Q3; whisker lengths indicate the 2nd and 98th percentiles.

on the differences in body size and our measured relationship between body size and number of neurons, we estimate that the difference in neuron count between these groups is approximately 2-fold (Figures 4D and 4E). Note that although the small and large populations have a 2-fold difference in the mean, the distributions do overlap due to the naturally occurring inhomogeneity in the small and large populations (Figure S3). Nevertheless, we expect that these groups would show differences in behavior if the thermal response were dependent on the number of neurons in the animal.

When we measured the calcium spike rates during thermal stimulation, we found a nearly identical temperature relationship in both small and large animals (Figure 4F), suggesting that *Hydra* maintain stable neural responses to thermal stimuli despite significant, 2-fold differences in the number of neurons. Both groups exhibit decreased calcium spike rates during negative thermal stimulation and increased calcium spike rates during positive thermal stimulation. Although some temperatures did show statistically significant differences between the thermal response of the "small" and "large" animals (Figure 4F), the effect size (δ) is small compared with the effect size of changes in stimulus temperature (e.g., δ = 0.96 when stimulating at 36°C when compared with culture temperature baseline; δ = 0.21 between large and small animals when stimulated at 36°C). At 9°C stimulation and control temperature (18°C), the effect size (δ) between the small and large groups was 0.66 and 0.67, respectively, which is comparable to the effect size of when comparing the calcium spike rate from the same animal measured on subsequent days (δ = 0.61, Figure S2).

Surgical removal of half of *Hydra*'s neurons does not significantly affect neural response to thermal stimulation

While animals with naturally occurring large and small nervous systems showed similar responses to thermal stimuli, we also wondered if this behavioral stability would apply to individual animals that had recently

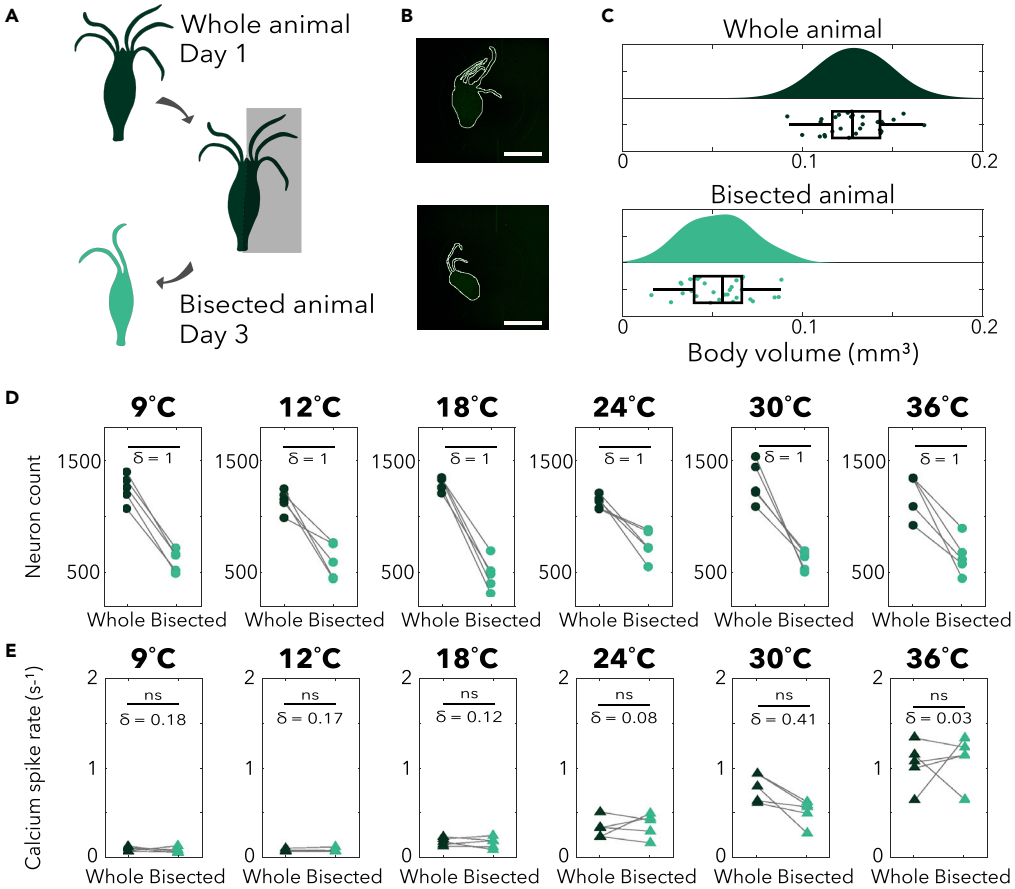

Figure 5. Changes in *Hydra*'s number of neurons due to surgical resection do not affect neural response to thermal stimulation, see also Figure S4

(A) Experimental schematic. A whole animal is imaged on Day 1 and then surgically resected, producing the bisected animal that is imaged on Day 3 (48–50 h after being cut).

(B) Representative image of whole *Hydra* (top panel), representative image of bisected *Hydra* (bottom panel). Scale bar, 1 mm.

(C) Size distribution of whole and bisected *Hydra*. (N = 5 per size at each stimulation temperature). Box-and-whisker plots indicate Q1, median, and Q3; whisker lengths indicate the 2nd and 98th percentiles.

(D) Comparison of neuron count between whole (N = 5 per size at each temperature) and bisected (N = 5 per size at each temperature) *Hydra*. The dark green data points on the left correspond to the number of neurons in the whole *Hydra*, which are connected to the corresponding bisected *Hydra*; the light green points on the right. δ, the effect size using Cliff's delta shown is calculated after bootstrapping with 100 iterations.

(E) Mean calcium spike rate comparison between whole and bisected *Hydra*. (ns = not significant, Wilcoxon signed-rank test. δ = Effect size using Cliff's delta).

suffered the injury of losing neural tissue. To answer this question, we cut the organisms in half along their oral-aboral axis. Thanks to *Hydra*'s radial symmetry and regenerative abilities, these surgically altered animals closed their wounds but did not regenerate to their original size within 48 h (Itayama and Sawada, 1995), yielding an animal with roughly half the number of neurons as the original whole (Figures 5A–5C, see transparent methods). Additionally, the radial symmetry helps to ensure that a resection along the oral-aboral axis does not remove the entirety of any one cell type (Javois et al., 1988; Wang et al., 2020). These resections are different from cuts normal to the oral-aboral axis that are known to produce significant behavioral deficits due to the removal of neuronal subtypes that are organized along the body column (Passano and McCullough, 1964). Given the radial symmetry of its nervous system and accompanying preservation of neuronal subtypes, it is a natural hypothesis that *Hydra* will maintain a level of stability when bisected along the oral-aboral axis. However, we could not find any reports quantifying the neural stability of bisected *Hydra*. Therefore, we set out to experimentally evaluate the stability of *Hydra*'s neural activity and behavior following injury.

By measuring neural responses to thermal stimulation both before and 2 days after this longitudinal resectioning, we could experimentally modulate the number of neurons in an organism and quantify resultant changes in neural activity patterns (Figure 5B-E). Specifically, we generated on average a 2-fold decrease in neuron count between whole and bisected *Hydra* (Figures 5C and 5D); however, we found that the neural response to thermal stimulation remained stable across all stimulus temperatures from 9°C to 36°C (Figure 5E). Namely, we found no statistically significant changes in the calcium spike rate when comparing *Hydra* before and after surgical resection of half of the animal's neurons (N = 5 animals per stimulus temperature). To account for naturally occurring variability between animals, we performed bootstrapping on the calcium spike rates within size groups and calculated the corresponding effect size (δ) for comparison (Figure S4). We found that the effect sizes between the calcium spike rates of whole and bisected *Hydra* are negligible to small ($\delta < 0.18$) for all stimulation temperatures except for 30°C and moderate ($\delta = 0.41$) for 30°C stimulation. These effect sizes are all small compared with the day-to-day variability within an animal ($\delta = 0.61$, Figure S2) and to the change in number of neurons, which has a maximum Cliff's delta of 1 (Figure 5D). Note that the surgical resection we chose, which cuts the animal along the oral-aboral axis, helps to preserve the diversity of cell types as cells differentiate along the oral-aboral axis (Siebert et al., 2019). Thus, these perturbations are expected to maintain all neuronal cell types. We would not necessarily expect that all potential resections (e.g., removing the oral or aboral ends of the animal) would show the same stable behavioral responses as we find in these experiments.

Evaluation of mechanisms of the tCB circuit

After finding that activity in *Hydra*'s tCB neurons changes according to the absolute temperature of an acute stimulus and is nearly invariant with neuron count, we asked what mechanism could link absolute temperature to these phenomena. We considered whether the simple hypothesis of diffusion coefficients' dependence on absolute temperature could explain elevated calcium spike rates (e.g., faster diffusion of ions and signaling molecules). The Stokes-Einstein equation states that diffusion coefficients are proportional to the absolute temperature of a system. The increase in the stimulus temperature from 18°C to 36°C corresponds to a 6.2% increase in absolute temperature and diffusion coefficients. However, we observe a nearly 800% increase in median calcium spike rate (Figure 3F). As observed changes in calcium spike rates are two orders of magnitude larger than changes in diffusion coefficient, the temperature-dependent increase in chemical diffusion is an unlikely mechanism for the observed relationship between *Hydra* neural activity and the absolute temperature of thermal stimuli.

As a more promising biophysical mechanism, we considered the temperature-dependent activity of the tCB neurons themselves, which can be quantified with the temperature coefficient, Q_{10}, a metric to describe the intrinsic thermal sensitivity of a system. As a point of reference, Q_{10} values greater than 2 indicate high temperature dependence, as has been described in studies on the effects of temperature on ion channel currents (Ito et al., 2015) and grasshopper sensory receptor neuron firing rates (Roemschied et al., 2014). This value can be calculated as a function of the rates of a process measured at two different temperatures (Equation 1).

$$Q_{10} = \left(\frac{R_2}{R_1}\right)^{\left(\frac{10°C}{T_2 - T_1}\right)} \quad \text{(Equation 1)}$$

We determine the value of Q_{10} for the tCB neurons to be 3.3 by measuring the slope of the log-linear relationship between rate ratio R_2/R_1 and temperature difference T_2-T_1 from our data of 18°C through 36°C in Figure 3F (see transparent methods). Performing similar calculations on calcium spike rates of *Hydra* cultured at 18°C or 25°C (Figure 3G) we found that Q_{10} is similar across different culture temperatures (Q_{10} = 3.09 for animals cultured at 18°C versus 3.45 for animals cultured at 25°C). These values of Q_{10} are within the range of values designated as thermosensitive in individual cells (Eisenman and Jackson, 1967; Binda et al., 2002; Ramot et al., 2008; Ito et al., 2015), which supports the hypothesis that the temperature sensitivity of the tCB neural firing rate may be a property of individual cells (which could be sensory or tCB neurons, see below) and that synchrony is achieved due to the *Hydra* peduncle's strong gap junctional coupling (Wolf et al., 2014).

It is important to note that although the Q_{10} value of the tCB neurons suggests they are highly temperature sensitive, they are likely not the primary thermosensory neurons. The onset of tCB calcium bursts was approximately 24 s (median value at 30°C stimulus) following thermal stimulation, a large time interval

given the hertz-scale frequency of tCB neurons after the start of firing and that the chamber temperature plateaus approximately 5 s after the start of the temperature change (median value at 30°C stimulus) (Figure S1). Instead, the long latency between the thermal stimuli and the neural activity suggests that the tCB neurons may be downstream of primary sensory neurons.

Furthermore, Hym-176A, C, and D-positive neurons that are primarily localized to the peduncle do not express clear homologs to thermosensitive ion channels like the TRPM or TRPA family (Peng et al., 2015; Malafoglia et al., 2016; McLaughlin, 2017; Klimovich et al., 2020). Instead, TRPM-like channels are expressed in pacemaker neurons in *Hydra*'s head region that control the regularity of spontaneous rhythmic contractions (Klimovich et al., 2020), whereas neurons associated with *Hydra*'s nematocytes express homologs for thermosensitive TRPA channels (Beckmann, 2013). These TRPM- and TRPA-expressing neurons are localized to *Hydra*'s hypostome and tentacles, a region known to contain broader types of sensory neurons (Bode et al., 1988; Koizumi et al., 1988), providing evidence that tCB neurons do not sense temperature directly. Qualitative examinations of tCB neurons' morphology (e.g., Videos S1 and S2) also support the idea of tCB neurons not being direct sensory neurons, with tCB neurons more closely resembling the compact shape of ganglion cells than the small narrow cell bodies of sensory neurons (e.g., as described in the basal disk ganglion cells of David [1973] or the multipolar neurons of Epp and Tardent [1978]).

Based on our data, we expect that the most likely explanation for the tCB neurons' temperature sensitivity is that individual cells in the tCB ensemble are downstream of other sensory neurons, supported by (1) extended latencies between thermal stimulus and tCB firing, (2) hypostome and tentacle localization of *Hydra* homologs to known thermosensitive channel genes, and (3) comparison of tCB neurons' morphology against that of known sensory neurons. The presented data are likewise consistent with a hypothesis that synchrony arises from gap junction coupling between radially symmetric neurons of *Hydra*'s peduncle. As initial support, *Hydra*'s genome contains gap junction proteins enriched in the peduncle (Alexopoulos et al., 2004; Chapman et al., 2010). For example, imaging data have validated the peduncle localization of the gap junction protein innexin-2, which is required for the normal synchronous activity of neurons that coordinate contraction bursts (Wolf et al., 2014). Similar gap junction proteins could likewise be responsible for the coordinated activity of tCB neurons, providing directions for future studies probing the circuit architecture of *Hydra*'s thermosensory response.

DISCUSSION

Unlike many invertebrate model systems like *C. elegans* and *Drosophila* that have stereotyped neural architectures with well-defined numbers of neurons, *Hydra*'s highly plastic nervous system, in conjunction with recent optical and genetic advances, facilitates studying how behaviors like sensory-motor responses are maintained as the number of neurons change under shifts like naturally-occurring size variation or oral-aboral resectioning. The two-layer microfluidic device shown here is a well-controlled method to study this process because it allows us to simultaneously image neural activity and behavior while we deliver thermal stimuli without mechanical stimulation artifacts. Using this technology, we found that when stimulated with a rapid temperature change, the animal first elongates and then contracts, with the peak body length occurring approximately 20 s after the stimulus onset. This behavioral response to a thermal stimulus is accompanied by synchronous periodic activity in a group of neurons near the animal's aboral end that we refer to as the tCB neurons. The frequency of tCB neuron activity, which we define as calcium spike rate, varies with the absolute temperature of the thermal stimulus, as opposed to relative changes from the baseline culture temperature. This relationship is maintained even if the number of neurons in the animal changes by a factor of 2 either by natural changes to the animal's size or by surgical resection along the oral-aboral axis.

Interestingly, neurons enriched in the peduncle do not express homologs for canonical thermoreceptors, but their large Q_{10} values ($Q_{10} > 3$) indicate a strong thermal dependence in these cells. These data suggest that either the tCB neurons are downstream of other sensory neurons or they express temperature-sensitive ion channels outside of the TRPA and TRPM family homologs that are found in other regions of the animal.

It bears emphasizing that the number of neurons changes naturally with animal size, so one may view the surgical resection and caloric restriction approaches as complementary methods of experimentally modulating the size of the animal and the number of neurons in the nervous system. Thanks to the gradual

adaptation enabled by caloric restriction and orientation of oral-aboral resectioning along *Hydra*'s radial axis of symmetry, we expect that these experimental perturbations allow for modulating neuron counts while not eliminating specific cell types. This feature allows us to independently modulate the number of neurons in the nervous system without significantly altering the overall structure of the nervous system. These features of *Hydra* are not true of other commonly used neuroscience model organisms (e.g., *C. elegans*, with its stereotyped number of neurons), underscoring *Hydra*'s value in studies on neural structures.

Although the radial symmetry of *Hydra* may lead one to expect that the surgical resections along the oral-aboral axis would not completely remove any neural structures, it is not yet known if there are neural specializations that could be removed from this manipulation. For example, the closely related cnidarian *Clytia hemisphaerica* is also radially symmetric, yet calcium imaging has found that spontaneous neural activity is not always radially symmetric (Weissbourd et al., 2021). Likewise, there are well-known left-right asymmetries in bilaterians including neurons that span both hemispheres that are important for mesoscale synchronization in computational simulations (Crick and Koch, 2005; Wang et al., 2017; Choi and Mihalas, 2019). In our experiments, we found no significant functional deficits following the oral-aboral resections suggesting that the neural circuits coordinating the response to thermal stimulation have no significant radial asymmetries in *Hydra*.

The ability to quantitatively study neural and behavioral activity as a function of nervous system size is one of the intriguing advantages of Hydra as a model organism. One potential future direction is to exploit this animal's ability to grow and shrink based on its environment, to study how organisms can dynamically regulate and reorganize their nervous systems based on satiety and nutrient availability. *Hydra* holds promise as a model organism for probing links between environmental conditions, internal signaling patterns, and mechanisms of homeostasis/regeneration. As we demonstrate in our work, the biochemical decision-making process of whether and which tissue to expand or sacrifice occurs while maintaining robust function to environmental stimuli. This provides means to repeatedly perturb *Hydra*'s size while studying the accompanying mechanisms for maintaining neural and behavioral homeostasis. With *Hydra*'s evolutionary similarity as the sister group to bilaterians and examples of other key body patterning mechanisms being conserved across evolution (e.g., Hox genes from *Drosophila*), we are enthusiastic for long-term efforts focused on uncovering *Hydra*'s intercellular signaling and computation mechanisms for adapting the nervous system to changes in body mass, as well as the mechanisms' applicability to broader species.

Future work is needed to confirm the molecular identity of the tCB neurons and understand the molecular mechanisms of the temperature response. Building on the quantitative input-output relationships established here across neural function and behavior, functional calcium imaging with cell type-specific labeling would help to identify molecular markers of the tCB sub-population and demonstrate relationships with previously defined neuron populations (e.g., CB neurons or clusters from single-cell RNA sequencing [scRNA-seq] datasets). The development of tools for cell type-specific labeling based on molecular identity would not only enable the identification of candidate proteins important in tCB neurons' functional activity (e.g., temperature-sensitive channels, gap junction proteins) but also open tremendous possibilities for perturbing tCB neurons' functionality (e.g., knockdown/knockin experiments).

Further work is also needed to fully elucidate the thermosensory response circuit. For example, modulating thermoreceptors with TRP agonists could help reveal their role in the circuit; computational algorithms for single-neuron tracking could enable us to directly measure the activity of neurons throughout *Hydra* to see which neurons precede or correlate with tCB activity, pointing toward upstream drivers (e.g., sensory neurons expressing TRP family homologs in *Hydra*'s tentacles). Similarly, blocking innexin-2 gap junction coupling could test if gap junctions indeed mediate the synchrony found in tCB activity.

Another remaining direction is how the tCB neurons maintain their thermal response properties in circuits of different sizes. The simplest explanation may be that the temperature sensitivity is a cellular property of specific neurons, such as other sensory neurons or tCB neurons expressing thermosensitive channels other than TRPA or TRPM family members; in this scenario, tCB neurons' activity could be synchronized by innexin-2 gap junction coupling. Alternatively, it is possible that *Hydra* have homeostatic mechanisms at the level of circuit connectivity to maintain a neural circuit architecture that has the same thermal response even as neurons are added and removed. For instance, *Hydra*'s radial symmetry ensures that no neuronal subtype is completely removed during surgical resectioning along the oral-aboral axis, potentially contributing to robust neural

response patterns following this perturbation in the number of neurons. It is also possible that the thermal response circuit is simply not affected by the overall number of neurons in the circuit, provided there is a critical minimum number of each constituent cell type. In principle, patch-clamp electrophysiology could provide insights into these possibilities. However, several features of *Hydra* have resulted in no successful patch-clamp experiments to date: in an intact *Hydra*, attempts to use an extracellular electrode to record activity from *Hydra*'s peduncle neurons were overwhelmed by electrical signals from accompanying muscle contractions (Dupre and Yuste, 2017), whereas *Hydra*'s flexibility and lack of endoskeleton present difficulties for holding a fixed position with intracellular recording electrodes (Taddei-Ferretti and Musio, 1999). And even for dissociated neurons, the fact that *Hydra* is a freshwater organism means that patch-clamp techniques must use low-ionic-strength media, which causes difficulty with successfully rupturing cell membranes and obtaining large signal-to-noise ratios (Santillo et al., 1997). As alternate approaches, blocking of cell-cell signaling or alteration of properties of neuronal subsets through cell type-specific promoters could help reveal if the stable behavioral response is a cellular-level or circuit-level property of *Hydra*.

Overall, *Hydra*'s combination of extreme neural plasticity and promise for genetically targeted manipulations could help evaluate the relative contributions of cellular and ensemble-level properties to the tCB circuit and its stability to perturbations in the number of constituent neurons. Additionally, by studying sensory-motor transformations like this thermal response, we may also learn about fundamental properties of neural circuits that are common to many species. For example, the tCB neurons show characteristics of a neural oscillator, which is a common motif across phylogeny, whereas mechanisms for selectively pruning or expanding the nervous system based on body mass (and environmentally driven conditions like satiety) could provide insights for robustly maintaining neural and behavioral function. These types of cross-species comparative studies could point toward conserved principles of neural circuits that appeared early in our evolutionary history. As described here, the ability to study neural and behavioral responses to thermal stimulation in a highly regenerative animal amenable to cellular-resolution fluorescence imaging offers many advantages as a model system for uncovering how neural circuits remodel without compromising their function.

Limitations of the study

One limitation of this study is that we cannot yet provide the precise molecular identity of the tCB neurons. Based on our calcium imaging data and how the location of the tCB neurons compares to *in situ* hybridization experiments, we are confident that the population is a subset of the CB neurons. However, *Hydra* still lacks established neuron-specific promoters, which makes it difficult for us to know the exact cell type. Fortunately, recent scRNA-seq studies in *Hydra* provide promise for CB neuron-specific markers (Siebert et al., 2019; Klimovich et al., 2020) suggesting that more accurate cell type identification will be possible in the near future. These new molecular techniques, combined with computational algorithms for single-neuron tracking, would enable future experiments to identify the role of each cell type in the types of sensory-motor behaviors studied here.

Resource availability

Lead contact

Information and requests for resources should be directed to and will be fulfilled by the lead contact, Jacob T. Robinson (jtrobinson@rice.edu).

Materials availability

This study did not generate new unique reagents.

Data and code availability

All data and code are available from the lead contact upon request.

METHODS

All methods can be found in the accompanying transparent methods supplemental file.

SUPPLEMENTAL INFORMATION

Supplemental information can be found online at https://doi.org/10.1016/j.isci.2021.102490.

ACKNOWLEDGMENTS

General: We would like to thank Dr. Christophe Dupre and Dr. Rafael Yuste (Columbia University), Dr. Celina Juliano (UC Davis) and Dr. Robert Steele (UC Irvine) for sharing transgenic *Hydra* lines, and Abby Primack (UC Davis) and Dr. Juliano for comments on the manuscript. Funding: This work was supported in part by the NSF IOS-1829158 and National Institutes of Health in the United States R21AG067034. C.N.T. is funded by a Fannie and John Hertz Foundation Fellowship and by a National Science Foundation Graduate Research Fellowship (1122374). K.N.B. is funded by training fellowships from the Keck Center of the Gulf Coast Consortia on the NSF Integrative Graduate Education and Research Traineeship (IGERT): Neuroengineering from Cells to Systems 1250104.

AUTHOR CONTRIBUTIONS

C.N.T. and S.K. performed and analyzed *Hydra* thermal stimulation experiments. K.N.B. performed and analyzed longitudinal imaging experiments on *Hydra*'s number of neurons as a function of body size. C.N.T., K.N.B., and B.W.A. designed, prototyped, and fabricated the microfluidic device. C.N.T., S.K., and B.W.A. implemented microcontroller automation of thermal stimulation experiments. C.N.T., J.T.R. supervised the research. C.N.T., S.K., K.N.B., and J.T.R. co-wrote the paper. All authors read and commented on the manuscript.

DECLARATION OF INTERESTS

The authors declare no competing interests.

Received: December 3, 2020
Revised: February 3, 2021
Accepted: April 27, 2021
Published: June 25, 2021

REFERENCES

Alexopoulos, H., Böttger, A., Fischer, S., Levin, A., Wolf, A., Fujisawa, T., Hayakawa, S., Gojobori, T., Davies, J.A., David, C.N., et al. (2004). Evolution of gap junctions: the missing link? Curr. Biol. *14*, R879–R880.

Alwes, F., Enjolras, C., and Averof, M. (2016). Live imaging reveals the progenitors and cell dynamics of limb regeneration. eLife *5*, e19766.

Ayaz, D., Leyssen, M., Koch, M., Yan, J., Srahna, M., Sheeba, V., Fogle, K.J., Holmes, T.C., and Hassan, B.A. (2008). Axonal injury and regeneration in the adult brain of Drosophila. J. Neurosci. *28*, 6010–6021.

Beckmann, A. (2013). Molecular factors of nematocyst morphogenesis and discharge in the freshwater polyp Hydra. https://doi.org/10.11588/heidok.00015956.

Binda, F., Bossi, E., Giovannardi, S., Forlani, G., and Peres, A. (2002). Temperature effects on the presteady-state and transport-associated currents of GABA cotransporter rGAT1. FEBS Lett. *512*, 303–307.

Bode, H., Berking S, David, C.N., Gierer, A., Schaller, H., and Trenkner, E. (1973). Quantitative analysis of cell types during growth and morphogenesis in Hydra. Wilhelm Roux Arch. Entwickl. Mech. Org. *171*, 269–285.

Bode, H.R., Heimfeld, S., Koizumi, O., Lttlefield, C.L., and Yaross, M.S. (1988). Maintenance and regeneration of the nerve net in Hydra. Am. Zool. *28*, 1053–1063.

Bosch, T.C., Krylow, S.M., Bode, H.R., and Steele, R.E. (1988). Thermotolerance and synthesis of heat shock proteins: these responses are present in Hydra attenuata but absent in Hydra oligactis. Proc. Natl. Acad. Sci. U S A *85*, 7927–7931.

Campbell, R.D. (1967). Tissue dynamics of steady state growth in Hydra littoralis. II. Patterns of tissue movement. J. Morphol. *121*, 19–28.

Campbell, R.D. (2008). Taxonomy of the European Hydra (Cnidaria: Hydrozoa): a re-examination of its history with emphasis on the species H. vulgaris Pallas, H. attenuata Pallas and H. circumcincta Schulze. Zool. J. Linn. Soc. *95*, 219–244.

Chapman, J.A., Kirkness, E.F., Simakov, O., Hampson, S.E., Mitros, T., Weinmaier, T., Rattei, T., Balasubramanian, P.G., Borman, J., Busam, D., et al. (2010). The dynamic genome of Hydra. Nature *464*, 592–596. https://doi.org/10.1038/nature08830.

Choi, H., and Mihalas, S. (2019). 'Synchronization dependent on spatial structures of a mesoscopic whole-brain network. PLoS Comput. Biol. *15*, e1006978.

Crick, F.C., and Koch, C. (2005). What is the function of the claustrum? Philos. Trans. R. Soc. Lond. B Biol. Sci. *360*, 1271–1279.

David, C.N. (1973). A quantitative method for maceration of hydra tissue. Wilhelm Roux Arch. Entwickl. Mech. Org. *171*, 259–268.

David, C.N., and Murphy, S. (1977). Characterization of interstitial stem cells in hydra by cloning. Dev. Biol. *58*, 372–383.

Dupre, C., and Yuste, R. (2017). Non-overlapping neural networks in Hydra vulgaris. Curr. Biol. *27*, 1085–1097.

Eisenman, J.S., and Jackson, D.C. (1967). Thermal response patterns of septal and preoptic neurons in cats. Exp. Neurol. *19*, 33–45.

Epp, L., and Tardent, P. (1978). The distribution of nerve cells inHydra attenuata Pall. Wilehm Roux Arch. Dev. Biol. *185*, 185–193.

Hammarlund, M., and Jin, Y. (2014). Axon regeneration in C. elegans. Curr. Opin. Neurobiol. *27*, 199–207.

Han, S., Taralova, E., Dupre, C., and Yuste, R. (2018). Comprehensive machine learning analysis of Hydra behavior reveals a stable basal behavioral repertoire. eLife *7*.

Itayama, T., and Sawada, Y. (1995). Development of electrical activity in regenerating aggregates of hydra cells. J. Exp. Zool. *273*, 519–526.

Ito, E., Ikemoto, Y., and Yoshioka, T. (2015). Thermodynamic implications of high Q 10 of thermo-TRP channels in living cells. Biophysics (Nagoya-shi) *11*, 33–38.

Javois, L.C., Bode, P.M., and Bode, H.R. (1988). Patterning of the head in hydra as visualized by a monoclonal antibody: II. The initiation and localization of head structures in regenerating pieces of tissue. Dev. Biol. *129*, 390–399.

Joven, A., Elewa, A., and Simon, A. (2019). Model systems for regeneration: salamanders. Development *146*, dev167700.

Juliano, C.E., Lin, H., and Steele, R.E. (2014). Generation of transgenic Hydra by embryo microinjection. J. Vis. Exp. e51888.

Kepner, W.A., and Hopkins, D.L. (1924). Reactions of Hydra to chloretone. J. Exp. Zool. *38*, 437–448.

Khetan, N., Maheshwari, S., and Athale, C.A. (2018). Quantitative detachment mechanics of Hydra from substrates. Proc. Indian Natl. Sci. Acad. *99*.

Klimovich, A., Giacomello, S., Björklund, Å., Faure, L., Kaucka, M., Giez, C., Murillo-Rincon, A.P., Matt, A.S., Willoweit-Ohl, D., Crupi, G., et al. (2020). Prototypical pacemaker neurons interact with the resident microbiota. Proc. Natl. Acad. Sci. U S A *117*, 17854–17863.

Koizumi, O., Heimfeld, S., and Bode, H.R. (1988). Plasticity in the nervous system of adult hydra. II. Conversion of ganglion cells of the body column into epidermal sensory cells of the hypostome. Dev. Biol. *129*, 358–371.

Malafoglia, V., Traversetti, L., Del Grosso, F., Scalici, M., Lauro, F., Russo, V., Persichini, T., Salvemini, D., Mollace, V., Fini, M., et al. (2016). Transient receptor potential melastatin-3 (TRPM3) mediates nociceptive-like responses in Hydra vulgaris. PLoS ONE *11*, 1–15.

Massobrio, P., Tessadori, J., Chiappalone, M., and Ghirardi, M.I. (2015). In vitro studies of neuronal networks and synaptic plasticity in invertebrates and in mammals using multielectrode arrays. Neural Plast. *2015*, 1–18.

Mast, S.O. (1903). Reactions to temperature changes in spirillum, Hydra, and fresh-water planarians. Am. J. Physiol. *10*, 165–190.

McLaughlin, S. (2017). Evidence that polycystins are involved in Hydra cnidocyte discharge. Invert. Neurosci. *17*, 1.

Murphy, T.H., and Corbett, D. (2009). Plasticity during stroke recovery: from synapse to behaviour. Nat. Rev. Neurosci. *10*, 861–872.

Nath, T., Mathis, A., Chen, A.C., Patel, A., Bethge, M., and Mathis, M.W. (2019). Using DeepLabCut for 3D markerless pose estimation across species and behaviors. Nat. Protoc. *14*, 2152–2176.

Noro, Y., Yum, S., Nishimiya-Fujisawa, C., Busse, C., Shimizu, H., Mineta, K., Zhang, X., Holstein, T.W., David, C.N., Gojobori, T., and Fujisawa, T. (2019). Regionalized nervous system in Hydra and the mechanism of its development. Gene Expr. Patterns *31*, 42–59.

Otto, J.J., and Campbell, R.D. (1977). Tissue economics of hydra. Regulation of cell cycle, animal size and development by controlled feeding rates. J. Cell Sci. *8*, 117–132.

Passano, L.M., and McCullough, C.B. (1963). Pacemaker hierarchies controlling the behaviour of hydras. Nature *199*, 1174–1175.

Passano, L.M., and McCullough, C.B. (1964). Co-ordinating systems and behaviour in Hydra: I. Pacemaker system of the periodic contractions. J. Exp. Biol. *41*, 643–664.

Peng, G., Shi, X., and Kadowaki, T. (2015). Evolution of TRP channels inferred by their classification in diverse animal species. Mol. Phylogenet. Evol. *84*, 145–157.

Ramot, D., MacInnis, B.L., and Goodman, M.B. (2008). Bidirectional temperature-sensing by a single thermosensory neuron in C. elegans. Nat. Neurosci. *11*, 908–915.

Roemschied, F.A., Eberhard, M.J., Schleimer, J.H., Ronacher, B., and Schreiber, S. (2014). Cell-intrinsic mechanisms of temperature compensation in a grasshopper sensory receptor neuron, *3*, R.L. Calabrese, ed. (eLife Sciences Publications, Ltd), p. e02078.

Rushforth, N.B. (1971). Behavioral and electrophysiological studies of Hydra. I. Analysis of contraction pulse patterns. Biol. Bull. *140*, 255–273.

Rushforth, N.B., Burnett, A.L., and Maynard, R. (1963). Behavior in hydra: contraction responses of hydra pirardi to mechanical and light stimuli. Science *139*, 760–761.

Santillo, S., Taddei-Ferretti, C., and Nobile, M. (1997). 'Resting potentials recorded in the whole-cell configuration from epithelial cells of Hydra vulgaris'. Ital. J. Zool. *64*, 7–11.

Schroeder, L.A., and Callaghan, W.M. (1981). Thermal tolerance and acclimation of two species of Hydra1. Limnol. Oceanogr. *26*, 690–696.

Scimone, M.L., Cote, L.E., and Reddien, P.W. (2017). Orthogonal muscle fibres have different instructive roles in planarian regeneration. Nature *551*, 623.

Shimizu, H., Sawada, Y., and Sugiyama, T. (1993). Minimum tissue size required for Hydra regeneration. Dev. Biol. *155*, 287–296.

Siebert, S., Farrell, J.A., Cazet, J.F., Abeykoon, Y., Primack, A.S., Schnitzler, C.E., and Juliano, C.E. (2019). Stem cell differentiation trajectories in Hydra resolved at single-cell resolution. Science *365*, eaav9314.

Song, Y., Ori-McKenney, K.M., Zheng, Y., Han, C., Jan, L.Y., and Jan, Y.N. (2012). Regeneration of Drosophila sensory neuron axons and dendrites is regulated by the Akt pathway involving Pten and microRNA bantam. Genes Dev. *26*, 1612–1625.

Szymanski, J.R., and Yuste, R. (2019). Mapping the whole-body muscle activity of Hydra vulgaris. Curr. Biol. *29*, 1807–1817.e3.

Taddei-Ferretti, C., and Musio, C. (1999). The neural net of hydra and the modulation of its periodic activity. In Lecture Notes in Computer Science (Including Subseries Lecture Notes in Artificial Intelligence and Lecture Notes in Bioinformatics), pp. 123–137.

Tatavarty, V., Torrado Pacheco, A., Groves Kuhnle, C., Lin, H., Koundinya, P., Miska, N.J., Hengen, K.B., Wagner, F.F., Van Hooser, S.D., and Turrigiano, G.G. (2020). Autism-associated Shank3 is essential for homeostatic compensation in rodent V1. Neuron *106*, 769–777.e4.

Technau, U., Cramer von Laue, C., Rentzsch, F., Luft, S., Hobmayer, B., Bode, H.R., and Holstein, T.W. (2000). Parameters of self-organization in Hydra aggregates. Proc. Natl. Acad. Sci. U S A *97*, 12127–12131.

Turrigiano, G.G. (2008). The self-tuning neuron: synaptic scaling of excitatory synapses. Cell *135*, 422–435.

Wang, Q., Ng, L., Harris, J.A., Feng, D., Li, Y., Royall, J.J., Oh, S.W., Bernard, A., Sunkin, S.M., Koch, C., and Zeng, H. (2017). Organization of the connections between claustrum and cortex in the mouse. J. Comp. Neurol. *525*, 1317–1346.

Wang, R., Steele, R.E., and Collins, E.-M.S. (2020). Wnt signaling determines body axis polarity in regenerating Hydra tissue fragments. Dev. Biol. *467*, 88–94.

Weissbourd, B., Momose, T., Nair, A., Kennedy, A., Hunt, B., and Anderson, D. (2021). Functional modules within a distributed neural network control feeding in a model medusa. bioRxiv.

Wittlieb, J., Khalturin, K., Lohmann, J.U., Anton-Erxleben, F., and Bosch, T.C. (2006). Transgenic Hydra allow in vivo tracking of individual stem cells during morphogenesis. Proc. Natl. Acad. Sci. U S A *103*, 6208–6211.

Wolf, A., Hwang, J.S., Wolf, A., Böttger, A., Shimizu, H., David, C.N., and Gojobori, T.I. (2014). Innexin gap junctions in nerve cells coordinate spontaneous contractile behavior in Hydra polyps. Sci. Rep. *4*, 1–8.

Wu, Z., Ghosh-Roy, A., Yanik, M.F., Zhang, J.Z., Jin, Y., and Chisholm, A.D. (2007). Caenorhabditis elegans neuronal regeneration is influenced by life stage, ephrin signaling, and synaptic branching. Proc. Natl. Acad. Sci. U S A *104*, 15132–15137.

Yamamoto, W., and Yuste, R. (2020). Whole-body imaging of neural and muscle activity during behavior in Hydra vulgaris: effect of osmolarity on contraction bursts. eNeuro *7*.

Yanik, M.F., Cinar, H., Cinar, H.N., Chisholm, A.D., Jin, Y., and Ben-Yakar, A. (2004). Functional regeneration after laser axotomy. Nature *432*, 822.

iScience, Volume *24*

Supplemental information

Hydra vulgaris shows stable responses to thermal stimulation despite large changes in the number of neurons

Constantine N. Tzouanas, Soonyoung Kim, Krishna N. Badhiwala, Benjamin W. Avants, and Jacob T. Robinson

Supplemental Data

Fig. S1. **Temperature profile and calcium trace of three representative *Hydra* stimulated at 30ºC, related to Fig. 3 and "Transparent Methods: Analysis of neural activity in the peduncle of *Hydra*"**

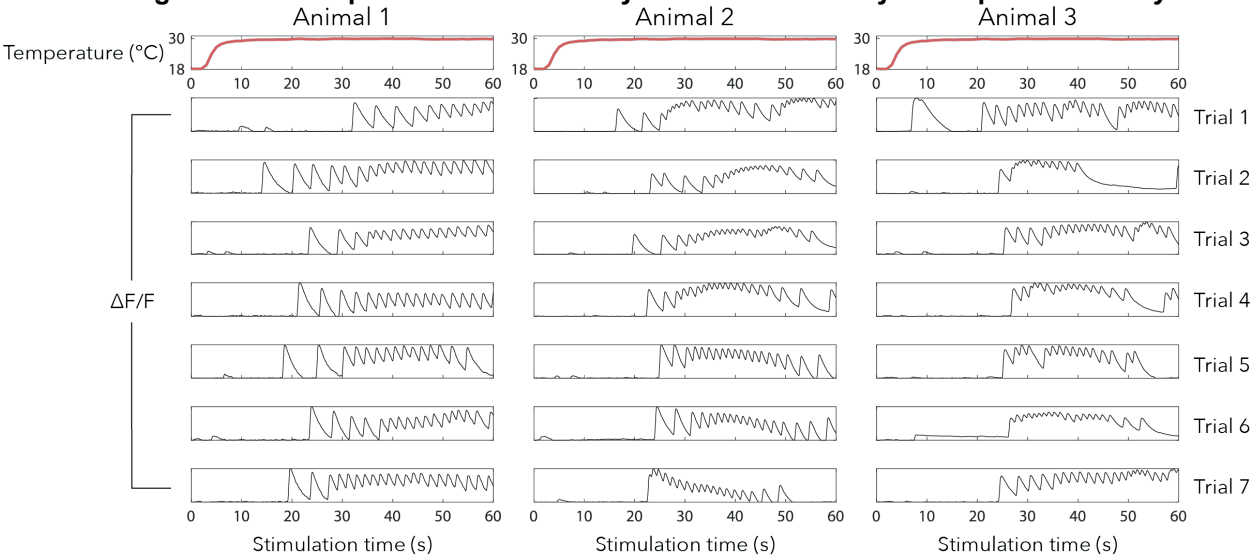

The temperature of the device plateaus approximately 5 seconds after the start of the temperature change, and the median time to the start of a contraction burst is 24 seconds after the start of the temperature change.

Fig. S2. **Day-to-day variation in intra-animal neural activity, related to Fig. 3**

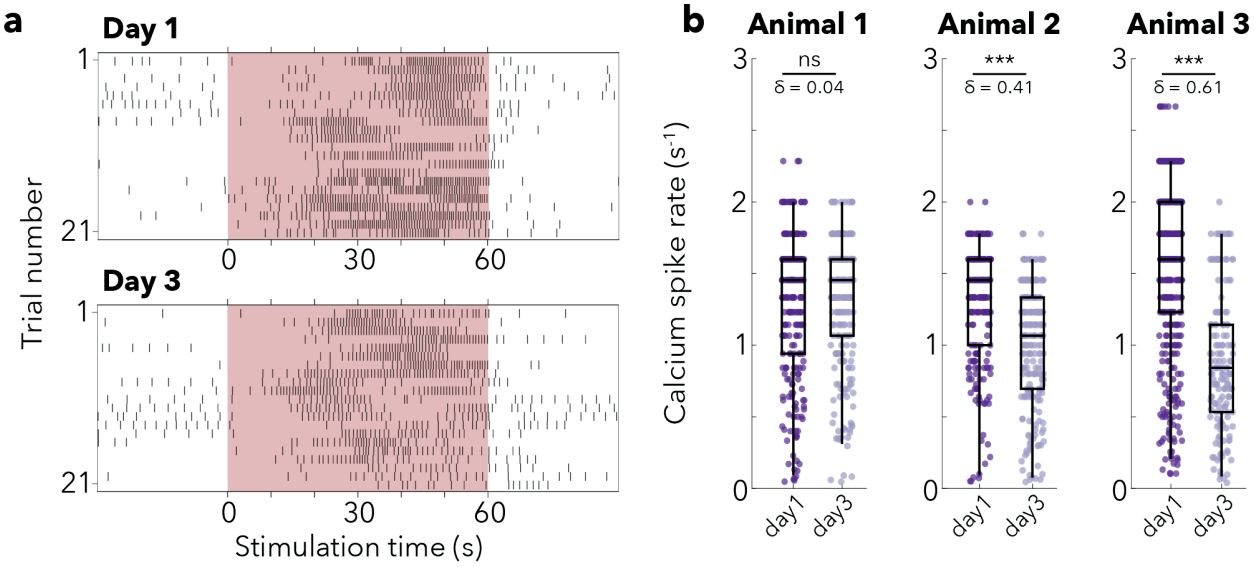

a Raster plot of *Hydra* stimulated at 36ºC on Day 1 and Day 3 (t = 48 hours after the previous stimulation on Day 1). **b** Calcium spike rate comparison between Day 1 and Day 3 for individual animals (Mann-Whitney U test, ns = not significant, *** p<0.0001, δ = Effect size using Cliff's delta). Box-and-whisker plots indicate Q1, median, and Q3; whisker lengths indicate the 2nd and 98th percentiles.

Fig. S3. **Differences in neuron counts due to *Hydra*'s natural size variations, related to Fig. 4**

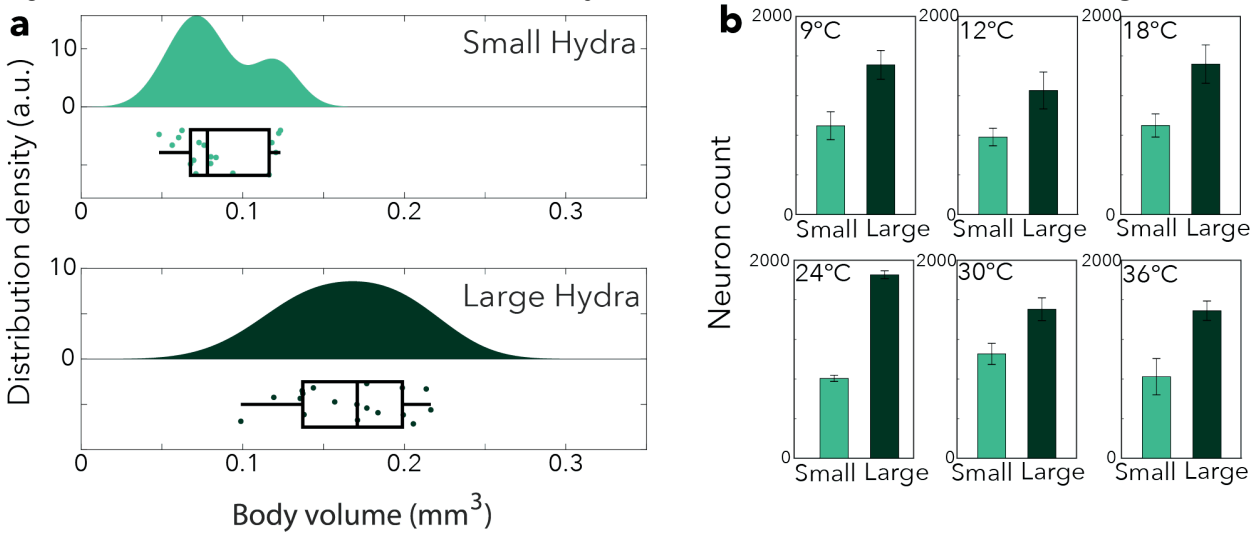

a Size distribution of small and large *Hydra*. Box-and-whisker plots indicate Q1, median, and Q3; whisker lengths indicate whisker lengths indicate the 2nd and 98th percentiles. **b** Comparison of neuron count between small and large *Hydra* groups at each stimulation temperature. (N=3 per size at each temperature). Data represented as mean +/- standard error of the mean.

Fig. S4. **Bootstrapping analysis on spike rates of whole and bisected Hydra, related to Fig. 5**

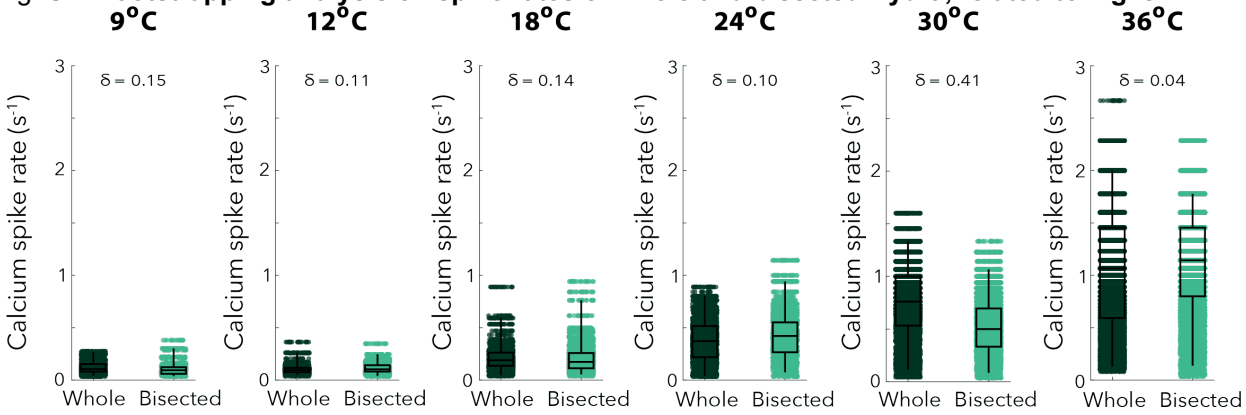

Comparison of bootstrapped calcium spike rates of whole and bisected *Hydra*. Box-and-whisker plots indicate Q1, median, and Q3; whisker lengths indicate whisker lengths indicate the 2nd and 98th percentiles.

Transparent Methods

Microfluidic device fabrication:

All microfluidic devices were fabricated using polydimethylsiloxane (PDMS) (Sylgard 184). The thermal stimulation chip is a two-layer device: bottom stimulus flow channels and a top *Hydra* immobilization chamber, separated by a glass coverslip. By separating *Hydra* from fluid flow, the animal can be rapidly heated/cooled (by flowing water at controlled temperatures through the bottom stimulus flow channels) without undesired mechanical stimulation from high flow rates (avoided due to the glass coverslip separation). To construct the double layer chip, we first fabricated the top immobilization layer by molding PDMS from a master mold adapted from a 2 mm diameter x 100 µm tall chemical perfusion chip (designed as previously described) (Badhiwala *et al.*, 2018). Briefly, a circular observation chamber designed specifically for *Hydra* was patterned using soft lithography on a silicon substrate, and a ~5mm thick layer of PDMS was molded from this master mold. After punching holes for the inlet and outlet ports with a 1.5mm diameter biopsy punch, the immobilization layer was O_2 plasma bonded to a 12mm diameter glass coverslip.

This top immobilization chip was then placed with a glass coverslip side facing down directly on the center of the master mold for the flow layer. Uncured PDMS was poured into the flow layer mold surrounding the immobilization chamber, taking care not to clog the ports in the immobilization layer. The master mold for the flow layer (adapted from Duret et al (Duret *et al.*, 2019)) was 3D-printed with 1mm tall channels (Form 2, Flexible Resin, Formlabs). After curing the PDMS for the bottom flow layer (thereby embedding the immobilization chamber), holes were punched for inlet/outlet access for the flow layer. Finally, this double layer microfluidic chip was O_2 plasma bonded to a 500 µm fused silica wafer (University Wafer).

After unloading *Hydra* from the device at the end of a trial (see "Loading and unloading *Hydra*"), both layers of the microfluidic device were rinsed with *Hydra* media (media adapted from the laboratory of Robert Steele), sonicated in *Hydra* media for at least 10 minutes, and soaked at room temperature in *Hydra* media. Such cleaning allowed for devices to be reused across multiple days of trials.

Hydra strains and maintenance:

All trials were conducted on transgenic lines with neuronal expression of GCaMP6s, developed with embryo microinjections by Christophe Dupre in the laboratory of Dr. Rafael Yuste. *Hydra* were cultured using the protocol adapted from the laboratory of Robert Steele (UC Irvine). *Hydra* were raised at either 18ºC or 25ºC in incubators, both with 12:12 hours of light:dark cycle. Animals were fed freshly hatched *Artemia* nauplii (Brine Shrimp Direct) three times a week and cleaned after approximately 4 hours with fresh *Hydra* media. All animals used in trials were starved for a day prior to thermal stimulation experiments and were not re-used.

Loading and unloading *Hydra*:

Hydra were loaded into the inlet port of *Hydra* enclosure using a 10 mL syringe with attached tygon tubing. *Hydra* were then pulled a couple of centimeters into the tygon tubing before the tubing was inserted into the inlet port of the microfluidic device. By applying gentle pressure and gently pulsing on the plunger of the syringe, *Hydra* could be successfully loaded into the immobilization chamber without damage from mechanical shear. After the experiments, *Hydra* were removed from the device by applying pressure on the plunger of a tygon tubing-attached syringe and flushing the organism out the outlet port.

Thermal stimulation assay

After loading *Hydra*, two programmable syringe pumps (New Era NE-500) controlled by an Arduino Mega ADK were used to drive the flow of deionized water at a rate of 6 mL/min through two inlet ports of the thermal stimulation device. The third inlet port was connected to an additional syringe (useful for removing air bubbles when initially filling the bottom stimulus flow channels prior to the start of a trial), and the device outlet port was connected to a water collection container. Fluid flow from the two pumps was heated/cooled using two in-line heaters (SC-20, Warner Instruments) regulated by a Dual Channel Bipolar Temperature Controller (CL-200A, Warner Instruments). One in-line heater supplied *Hydra*'s culture temperature during control periods (i.e. 18°C or 25°C), while the other heater supplied the desired stimulus temperature of a given trial (i.e. 9°C, 12°C, 18°C, 24°C, 25°C, 30°C, or 36°C). To compensate for heat exchange between water flowing through inlet tubing and the environment, a FLIR ONE thermal camera

was used to calibrate the relationship between in-line heater temperature settings and actual temperatures of the thermal stimulation device.

Each thermal stimulation trial began with two minutes at *Hydra*'s culture temperature. Subsequently, the trial alternated between stimulus periods (single temperature for a given trial; 9°C, 12°C, 18°C, 24°C, 25°C, 30°C, or 36°C) and control periods (based on *Hydra*'s culture temperature; 18°C or 25°C). Stimulus periods always lasted for 60 seconds, while control periods varied in length between 30 and 90 seconds in 15 second increments, to help distinguish between stimulus-evoked responses and spontaneous activity. The lengths of control periods were randomly ordered and averaged to 60 seconds over the course of a trial. For a visual representation of thermal stimulation protocols, see Fig. 3a. The timing of transitions between stimulus and control periods were recorded through the Arduino's Serial Monitor (57600 baud rate) and used to determine portions of recordings corresponding to stimulus and control periods. For experiments on size comparison of *Hydra* cultured at 18°C, 3 large and 3 small animals for each temperature (9°C, 12°C, 18°C, 24°C, 30°C, and 36°C), 36 animals in total were used. For *Hydra* cultured at 25°C, 3 animals were used at 18°C, and 4 animals at 25°C, 30°C, and 36°C over the course of 7 days.

Fluorescence imaging for GCaMP6s was conducted on a Nikon SMZ18 stereomicroscope with a SHR Plan Apo 2x objective (0.3 NA) and Andor Zyla 4.2 (16 fps, 3x3 image binning). Excitation was provided by a X-Cite Xylis XT720L at 50% intensity through a Chroma EGFP filter cube (catalog no. 49002). The start of fluid flow using Arduino and the start of recording using Andor Solis were manually synced with a maximum delay less than 0.5 seconds.

Measuring Day-to-Day Variability in Calcium Spike Rate

To better understand the source of variability in our data we asked how much of the difference in calcium spike rates could be explained by day-to-day variability in the same animal. To answer this question, we stimulated the same whole *Hydra* twice at 36°C over a 48 hours interval (N=3 organisms) - the same time interval between the whole and partial *Hydra* experiments. We found that while one animal maintained its spike rate with no statistically significant difference, two animals had a statistically significant decrease in spike rate, even when stimulated at the same temperature before and after the 48-hour difference (Fig. S2b). Accompanying effect sizes measured using Cliff's delta (δ) ranged from 0.04 for first animal to 0.41 and 0.61 for the latter two (overall pooled effect size of 0.35), contextualizing the relative magnitudes of observed experimental effects against typical day-to-day variability in *Hydra*.

Longitudinal imaging of the entire nervous system

Transgenic *Hydra vulgaris* AEP expressing GFP (green fluorescent protein) in their interstitial cell lineage were used to investigate how the number of neurons varies with animal size and nutrient availability. Animals with large body size (>2 mm long) at the beginning of the study were starved for the duration of the experiment. A control group of animals with small body size (< 1mm) at the beginning of the study were fed with an excess of freshly hatched *Artemia nauplii* three times a week. Size of the animal was defined as the length of the animal in a relaxed state (between fully contracted and fully elongated). *Hydra* media was replaced daily for all animals.

Volumetric imaging was performed using a confocal microscope (Nikon TI Eclipse) with animals immobilized in chemical perfusion microfluidic chips (see Badhiwala et al. (Badhiwala *et al.*, 2018)) and chemically paralyzed with 1:5000 linalool. Animals were imaged three times a week (one day after the control animals were fed) over two weeks. All images were acquired with a 10x DIC objective. The majority of the images were acquired with 1024 x 1024 pixels (x, y) resolution and 5 mm z-resolution. A lower resolution of 512 x 512 pixels and 10 mm z-resolution were used in a few cases to speed up volumetric imaging where micromotions of the animals could not be completely eliminated with chemical anesthetic (becoming increasingly important with animals starved for extended periods of time).

To quantify the total number of neurons, a maximum intensity projection image was generated from the z-stacks. After binarizing the resulting image with a user-defined threshold, individual regions (or neurons) were summed to determine the total number of neurons. However, due to anatomical overlap of multiple neurons in high-density regions such as the peduncle, future work will focus on developing transgenic animals that express fluorescent reporters in the nuclei of specific neural cell types, rather than in the cytosol of interstitial cell derived lineages (as in the animals used here).

To quantify the body size during an experiment, we binarized the maximum intensity projection image with a lower threshold than above. Filling holes in the binarized image produced the binary mask for

the whole animal. Body size was calculated as the area of this binary region, and body volume was body size times the thickness of the immobilization chamber (160 μm).

The duration of the experiment was kept under two weeks, as well-fed animals can reproduce asexually by budding every 3-4 days. In fact, one of the animals in the well-fed group began forming a bud on day 10 of the experiment. Additionally, as animals are starved, they become smaller and more transparent, making them difficult to handle. In our starved group, we 'lost' one of the animals on day 15 as it was either too transparent or had shrunk considerably to not be discerned from the plate.

Creating bisected *Hydra*

For the purpose of investigating whether the number of neurons affect the neural response to thermal stimulation in *Hydra*, the animals were cut along the oral - aboral axis in order to ensure we have a significantly different distribution of body size while retaining tentacles, the hypostome, body column, and peduncle. Whole, uncut *Hydra* were imaged on day 1 as the same protocol described above. Then each *Hydra* was cut along the oral-aboral axis under a dissection microscope using an X-acto knife (#2 knife with #22 blade). The cut animals were incubated in separate 24-well compartments and were fed the day after being cut (day 2) to keep the feeding schedule consistent. After letting them recover for 48 to 50 hours, they were thermally stimulated again under the same condition they were exposed to before being cut. Five animals were used for each stimulation temperature. For the comparison of neural response between whole and bisected *Hydra*, only one of the two bisected *Hydra* was used.

Behavioral analysis

DeepLabCut (Nath *et al.*, 2019) along with custom MATLAB code was used to quantify *Hydra*'s behavioral responses to thermal stimuli. 20 frames per video were extracted for manual tracking according to k-means clustering on DeepLabCut. *Hydra* in each frame was then manually annotated with the locations of the basal disc (aboral end), left side, center, and right side of the body, and hypostome (oral end). Two corners of the immobilization chamber were additionally annotated, providing a known distance (2 mm) to convert pixel measurements to micrometer measurements. The annotated dataset was used as training data for DeepLabCut. After evaluating the model, the videos were analyzed using the trained model which yielded the coordinates of the seven points listed above for every frame (total of 14,600 frames) for every video, along with annotated videos. With the coordinates obtained from DeepLabCut annotations, body width was calculated as the sum of the distance from the left side to the middle of the body and the distance from the middle to the right side of the body, and body length was calculated as the sum of the distance from the hypostome to the middle of the body and the distance from the middle of the body to the basal disc (Fig. 2b, bottom panel) with a custom MATLAB code.

Analysis of neural activity in the peduncle of *Hydra*

To determine the timing and frequency of calcium spikes in *Hydra*'s peduncle oscillator, fluorescence microscopy recordings from thermal stimulation trials of neuronal GCaMP6s *Hydra* (see "Thermal Stimulation Assay") were processed in Fiji (ImageJ) (Schindelin *et al.*, 2012) and in MATLAB. For each frame of the recording, Fiji was used to calculate the average intensity of a ROI encompassing *Hydra*'s peduncle and aboral regions (same ROI for the entire recording). In MATLAB, this intensity trace was smoothed (5 data point span), and the built-in findpeaks function was used to determine calcium spike locations based on their prominence in the intensity traces (see Movie S1, Movie S2, and Fig. S1 for representative calcium traces). Spurious spikes (e.g. from measurement noise) were eliminated by additionally testing that each identified calcium peak was the only local maximum exceeding a threshold prominence value within a narrow window of the peak.

Raster plots were then directly produced from the times of peduncle oscillator spikes during each stimulus period and the surrounding 30 seconds at culture temperature. Peristimulus time histograms (defined as calcium firing rate) were calculated by counting the number of spikes across all stimulus periods at a given stimulation temperature in a 10-second sliding window, then normalizing by the number of stimulus periods and the length of the window. Instantaneous calcium spike rates for a given thermal stimulus temperature were defined as the inverse of the amount of time elapsed between two successive calcium spikes during stimulus periods. We highlight that apparent discretization of instantaneous calcium spikes at high rates stems from discrete sampling intervals (i.e., frames in a microscopy video) to measure a continuous underlying process (i.e., calcium dynamics in a GCaMP6s-expressing neuron). At these relatively high firing rates, a small integer number of frames elapsed between peaks would cause apparent

discretization of a continuous process. For instance, 8 frames elapsed between spikes in a 16 fps recording would correspond to a calcium spike rate of 2/sec. The next slowest measurable increment 16 fps would be a calcium spike rate of 1.78/sec, arising from 9 frames elapsed between spikes, and so on for other integer counts of elapsed frames.

Estimating the value of Q_{10} of tCB neurons

The thermal coefficient, Q_{10}, was calculated to elucidate one possible biophysical mechanism behind the temperature dependent calcium spike rates using Eq. 1 (see Evaluation of mechanisms of the temperature-dependent calcium spike rate in Results). T_1 is 18ºC, and R_1 is the median calcium spike rate at T_1. T_2 ranges from 18ºC to 36ºC, and R_2 is the corresponding median calcium spike rate at T_2. As the nature of Eq. 1 is in the form of an exponential, we took log in the y axis, plotting a log-linear plot of $\log(R_2/R_1)$ vs. (T_2-T_1). Using the polyfit function in MATLAB, we fitted the data points to a linear equation to determine the slope. The value of Q_{10} was then calculated using the obtained slope.

Statistical analysis

To determine statistical significance between the calcium spike rates across temperatures, two-sided Wilcoxon rank sum test (equivalent to Mann-Whitney U-test) was implemented using the ranksum function in MATLAB. The test returns the p-value with the null hypothesis that the data points in the two datasets to be samples from distributions (whether continuous samples, or discrete and ordinal samples) with equal medians (Lehmann, 1951; Fay and Proschan, 2010). This test also allows the two data sets to have different lengths. This particular test was chosen because of the nature of length-variant distribution of calcium spike rates, of which we consider the median, not the mean, for comparison.

We also used Cliff's delta (Cliff, 1993), which represents the effect size that gives a quantitative measurement of the difference between two groups of data. We chose to use Cliff's delta because of its neutrality to mean values, as it takes the entire distribution into account. Let $X = \{x_1, \ldots, x_m\}$ and $Y = \{y_1, \ldots, y_n\}$ be the two samples of interest. Defining d as follows,

$$d(i,j) = \begin{cases} +1, & x_i > y_j \\ -1, & x_i < y_j \\ 0, & x_i = y_j \end{cases}$$

Cliff's delta (δ) can be calculated as

$$\delta = \frac{1}{mn} \sum_{i=1}^{m} \sum_{j=1}^{n} d(i,j)$$

where $-1 \leq \delta \leq +1$. The absolute δ values that are closer to 1 indicate larger differences between the samples, while the values closer to 0 indicate small differences between the samples.

We also performed statistical bootstrapping to randomly pool distributions of calcium spike rates from whole and bisected Hydra (N=5) in order to quantify statistical difference between the two groups. As per protocol (see "Thermal stimulation assay" in Transparent Methods), each animal was stimulated 7 times at a given temperature. We pooled calcium spike rates from 7 stimulation periods across the aforementioned 5 animals to create one artificial animal so that at least one stimulation period from each of the animals would be included. This process was done 100 times to create the calcium spike rates shown in the Fig. S3.

Supplemental References

Badhiwala, K. N. et al. (2018) 'Microfluidics for electrophysiology, imaging, and behavioral analysis of: Hydra', *Lab on a Chip*. Royal Society of Chemistry, 18(17), pp. 2523–2539. doi: 10.1039/c8lc00475g.
Cliff, N. (1993) 'Dominance statistics: Ordinal analyses to answer ordinal questions.', *Psychological Bulletin*, 114, pp. 494–509.
Duret, G. et al. (2019) 'Magnetic Entropy as a Proposed Gating Mechanism for Magnetogenetic Ion Channels', *Biophysical Journal*. Cell Press, 116(3), pp. 454–468. doi: 10.1016/J.BPJ.2019.01.003.
Fay, M. P. and Proschan, M. A. (2010) 'Wilcoxon-Mann-Whitney or t-test? On assumptions for hypothesis tests and multiple interpretations of decision rules', *Statistics surveys*, 4, pp. 1–39. doi: 10.1214/09-SS051.
Lehmann, E. L. (1951) 'Consistency and Unbiasedness of Certain Nonparametric Tests', *The Annals of Mathematical Statistics*. Institute of Mathematical Statistics, 22(2), pp. 165–179. Available at: http://www.jstor.org/stable/2236420.
Nath, T. et al. (2019) 'Using DeepLabCut for 3D markerless pose estimation across species and behaviors', *Nature Protocols*, 14(7), pp. 2152–2176. doi: 10.1038/s41596-019-0176-0.
Schindelin, J. et al. (2012) 'Fiji: an open-source platform for biological-image analysis', *Nature Methods*, 9(7), pp. 676–682. doi: 10.1038/nmeth.2019.